ChemComm

COMMUNICATION

View Article Online
View Journal

Cite this: DOI: 10.1039/d6cc00930a

Received 11th February 2026,
Accepted 16th February 2026

DOI: 10.1039/d6cc00930a

rsc.li/chemcomm

Coordination cages as tunable ligands for the synthesis of porous salts

Qiong Zhou,[a] Nobuyuki Yamamoto,[a] Dewni D. Fernando,[a] Yaroslav Losovyj,[ab] Alex Lovstedt [a] and Eric D. Bloch *[a]

Zirconium-based coordination cages are versatile platforms for exploring host–guest chemistry and the design of advanced materials. In this work, we report the synthesis and characterization of a zirconium coordination cage featuring a sulfonate-based binding pocket preorganized for metal cation coordination. Through careful control of synthetic conditions, we selectively prepare cage variants incorporating lithium, sodium, or an empty binding pocket. Post-synthetic modification enables precise metallation with alternative metal cations. This work highlights the utility of preorganized coordination environments in designing tunable porous materials and provides new strategies for the synthesis of customizable porous salts.

Permanently porous coordination cages have emerged over the past decade as highly tunable molecular materials with significant utility as solid-state adsorbents.[1,2] A subset of these porous cages exist as charged species due to variations in metal–ligand stoichiometry,[3] ligand functionalization,[4,5] or post-synthetic modification.[6] Practically, the charged nature of these cages has been leveraged in ion exchange routes to purify or optimize surface areas,[7,8] as well as in mass spectrometry-based characterization methods.[9] More recently, charged coordination cages have been employed in synthesizing porous salts-solids composed of porous ions paired with complementary charged species, which may themselves be porous or nonporous.[10–14]

Our group has reported various porous salts composed of two oppositely charged coordination cages.[15] Recent studies have significantly expanded this approach by pairing a single porous ion with a charge-balancing species possessing intrinsic reactivity or photochemical properties. For instance, polyoxometalate (POM)-based porous salts have been synthesized by replacing nonporous counter-cations in POM samples with porous cages,[16,17] resulting in catalytically active solids wherein catalytic activity originates from the POM and porosity from the cage. Similarly, Le Ouay and coworkers demonstrated enhanced enzymatic activity through charge-driven self-assembly of enzymes into porous frameworks.[18] Our group recently illustrated the utility of pairing mononuclear transition metal complexes with porous cages,[19] yielding porous salts with cage-derived porosity and complex-derived reactivity. Additionally, we reported a strategy where otherwise neutral cages bind halide ions at open metal sites, thereby forming porous salts from initially nonporous salts, with counter-cations that could either be nonporous (*e.g.*, tetrabutylammonium) or porous molecules.[10]

To further expand the synthetic toolkit available for porous material researchers, we sought to develop complementary cation-binding cages capable of transforming nonporous salts into porous materials. A wide range of functionalized organic ligands have been incorporated into cage formation, with additional functional groups serving as binding sites for metal ions *via* pre-synthesis ligand designs and post-synthetic modifications.[20–26] For example, pyridyl and bipyridyl-containing ligands are commonly used for this purpose.[27–29] In these systems, the cage is formed by carboxylate groups that coordinate with the Zr_3Cp_3 cluster, while the bipyridyl groups bind Pd(II)[30,31] or Pt(II).[32] The introduction of these secondary metal ions imparts unique optical and catalytic properties to the cage. However, in such cases, Pd(II) and Pt(II) are typically also coordinated by other anions, most often Cl^- depending on the metal source added.[25,33] Therefore, the addition of these secondary metal ions does not alter the net charge of the original cage. Unlike cages that become charged upon halide-binding, which rely on metal paddlewheel units, a distinct synthetic approach was necessary for cages capable of binding metal cations.[10,34,35] We identified a recently reported cage structure with strategically positioned sulfonate groups capable of metal cation binding. The structure demonstrates sodium cation binding at half of the available sites within its reported crystal structure, making it a promising platform for synthesizing novel cation-binding porous cages.

[a] *Department of Chemistry, Indiana University, Bloomington, Indiana 47405, USA. E-mail: edbloch@iu.edu*
[b] *Department of Physics and Astronomy, University of Nebraska, Lincoln, Nebraska 68588, USA*

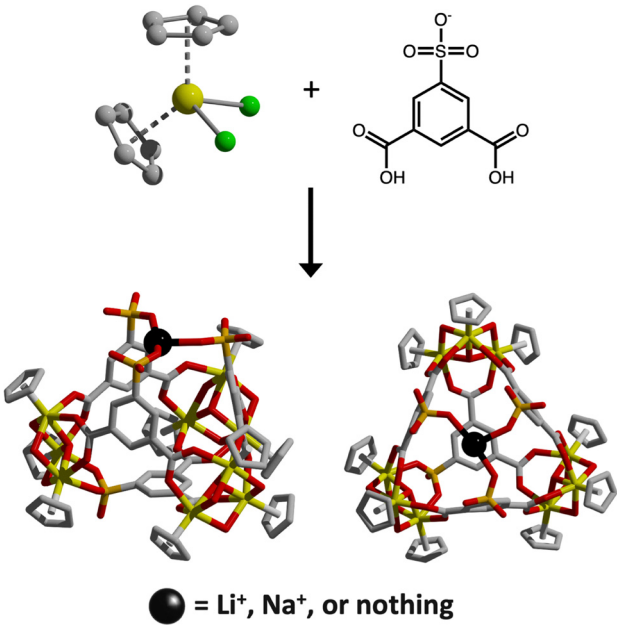

Fig. 1 The reaction of zirconocene dichloride with 5-sulfoisophthalic acid affords a porous zirconium cage $[(Zr_3(\mu_3\text{-}O)(\mu_2\text{-}OH)_3Cp_3)_3(5\text{-}SO_3\text{-}bdc)X]$ where the sulfonate binding pocket can feature an alkali metal cation or remain empty for subsequent cation binding.

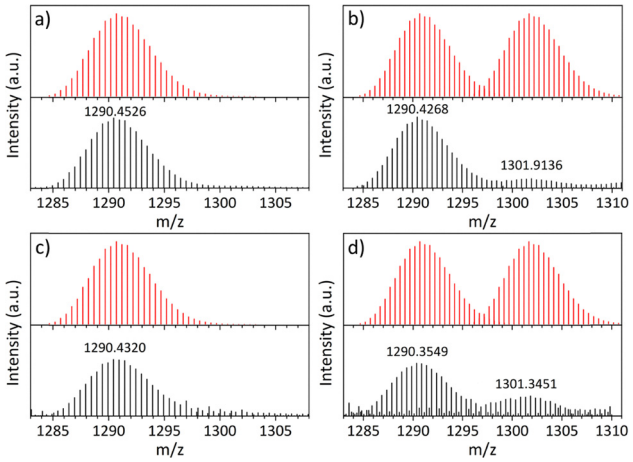

Fig. 2 Mass spec of free-pocket cage (a), Na-bound cage (b), Li-bound (c), and free-pocket cage + NaCl (d) which agreed with simulated spectra pattern (red traces). In simulation, the first peak corresponds to doubly-protonated free-pocket cage with a formula of $H_2[(Zr_3(\mu_3\text{-}O)(\mu_2\text{-}OH)_3Cp_3)_3(5\text{-}SO_3\text{-}bdc)_4]$ and the second peak corresponds to Na^+-adduct of protonated free-pocket cage with a formula of $HNa[(Zr_3(\mu_3\text{-}O)(\mu_2\text{-}OH)_3Cp_3)_3(5\text{-}SO_3\text{-}bdc)_4]$.

Du and coworkers reported the synthesis of the zirconium-based cage *via* the reaction of the sodium salt of 5-sulfoisophthalic acid with zirconocene dichloride in acetonitrile (MeCN).[36] The resulting material $[(Zr_3(\mu_3\text{-}O)(\mu_2\text{-}OH)_3Cp_3)_3(5\text{-}SO_3\text{-}bdc)_4Na_{0.5}]Cl_{0.5}$ features a tri-sulfonate binding pocket with partial sodium occupancy. We reasoned that this equilibrium binding could be shifted to afford cages with tunable M^+ occupancy, including a cation-free variant that could subsequently bind alkali metal cations from salts of interest.

Although we were unable to reproducibly access a cage with 50% NaCl loading, modification of the reported synthesis by increasing water content and shortening reaction times afforded a solid with full NaCl occupancy. Single-crystal X-ray diffraction revealed a composition of $[(Zr_3(\mu_3\text{-}O)(\mu_2\text{-}OH)_3Cp_3)_3(5\text{-}SO_3\text{-}bdc)_4Na]Cl$, consistent with full occupancy of Na^+ within the sulfonate pocket (Fig. 1). The cage consists of three Zr_3Cp_3 clusters coordinated by four 5-SO_3-bdc ligands, with the uncoordinated sulfonate groups converging to define the binding pocket.

Bulk characterization supports this formulation. ^{1}H NMR spectroscopy shows a Cp–H: aromatic–H ratio of approximately 45 : 12 (Fig. S18), and XPS analysis indicates a Zr : Na : Cl ratio of approximately 9 : 1 : 1 (Tables S2, S5 and Fig. S11), both consistent with the assigned composition. Electrospray ionization mass spectrometry of samples dissolved in methanol exhibits dominant peaks at 1290.4268 and 1301.9136 *m/z*, corresponding to the free cage cation (loss of Na^+) and the Na^+-bound form, respectively (Fig. 2b). The predominance of the free cage under these conditions is consistent with competitive coordination by methanol.

As expected for zirconium-based porous materials, the cage appeared stable up to 350 °C under simulated air atmosphere (80% N_2, 20% O_2) as indicated by TGA analysis (Fig. S32).[37] Activation at room temperature (RT) was sufficient to give porous solid with a BET surface area of 635 $m^2\ g^{-1}$ (Fig. 4c), which is significantly higher than the value of 289 $m^2\ g^{-1}$ for the previously reported system.[36] Gas uptake measurements were first used to confirm accessibility of the internal cavity to larger molecules, providing a foundation for subsequent solid-state cation binding studies. Adsorption measurements at 298 K revealed that the cage is porous to small molecules such as CO_2 (330 pm), CH_4 (380 pm), Xe (396 pm), C_3H_8 (430 pm), and *n*-butane (500 pm), with respective uptakes of 7.59, 0.39, 1.16, 3.68, and 2.49 mmol g^{-1} at 1 bar (Fig. S33).

Because use of the sodium salt of 5-SO_3-H_2bdc$^-$ reproducibly afforded cages with an occupied sulfonate binding pocket, we explored alternative routes to access a cage with reduced or absent alkali-metal occupancy. These efforts focused on substitution of the ligand counterion and on the use of alkali-metal complexing agents introduced either during or after cage synthesis. Using 5-SO_3Li-H_2bdc in place of 5-SO_3Na-H_2bdc as the bridging ligand afforded a Li-bound cage that crystallized as small, needle-like crystals, which were notably more fragile than their Na-bound counterparts. The resulting material, formulated as $[(Zr_3(\mu_3\text{-}O)(\mu_2\text{-}OH)_3Cp_3)_3(5\text{-}SO_3\text{-}bdc)_4Li{\cdot}MeCN]Cl$, adopts the same overall cage connectivity as the Na-bound analogue featuring a tri-sulfonate binding pocket occupied by Li^+ (Fig. 1 and Fig. S2).

Since substitution of the alkali metal counterion alone did not reliably afford a cage with a vacant sulfonate binding pocket, we turned to the use of chelating agents to remove Na^+ prior to cage formation. To this end, 15-crown-5 was added to the Na-bound cage reaction mixture before heating, with the expectation that Na^+ would be preferentially sequestered by the crown ether rather than occupying the tri-sulfonate pocket.

This strategy reproducibly yielded a cage featuring a vacant tri-sulfonate binding site, formulated as $[(Zr_3(\mu_3\text{-}O)(\mu_2\text{-}OH)_3Cp_3)_3(5\text{-}SO_3\text{-}bdc)_4]$, and denoted hereafter as the free-pocket cage (Fig. 1 and Fig. S3). Both electrospray ionization mass spectrometry and XPS confirm the absence of Na^+ in the isolated material (Fig. 2a and Fig. S13). Upon activation at room temperature, the free-pocket cage is highly porous to N_2, with a BET surface area of 576 $m^2\ g^{-1}$, comparable to that of the Na-bound cage. By contrast, the Li-bound cage remains porous to N_2 but exhibits a substantially lower BET surface area of 213 $m^2\ g^{-1}$ and reduced uptake of other gases relative to the Na-bound analogue (Fig. 4c).

Encouraged by the confirmed porosity and accessibility of the sulfonate binding pocket, we next examined whether metal cations could be introduced into the free-pocket cage under post-synthetic, solid-state conditions. Treatment of the free-pocket cage with a methanolic solution of NaCl resulted in incorporation of Na^+, as confirmed by both electrospray ionization mass spectrometry and XPS (Fig. 2d and Fig. S14). These results establish that the vacant tri-sulfonate pocket remains chemically accessible in the solid state and can bind external cations delivered from simple inorganic salts. More compelling opportunities arise when alkali metal binding is used to pair the porous scaffold with anions that impart optical, catalytic, or gas-binding properties, while the cage provides permanent porosity and structural stability.

As an example of pairing the porous Zr cage with an optically active counter-anion, we examined the incorporation of sodium ions delivered from Eosin Y disodium salt (Eosin Y). Mixing the free-pocket cage with Eosin Y in MeCN yielded orange–pink solids that exhibited yellow fluorescence under 365 nm UV irradiation (Fig. S44), consistent with the presence of the dye. Importantly, porosity was retained following post-synthetic treatment: after activation at room temperature, the resulting material displayed an N_2-accessible BET surface area of 419 $m^2\ g^{-1}$ (Fig. 4d).

Quantitative analysis by XPS indicates a Br : Zr ratio and Na : Zr ratio corresponding to approximately 0.22 dye molecules per cage, equivalent to ~44% occupancy of the tri-sulfonate binding pockets by Na^+ (Fig. S15). Similar Eosin Y content in the formed salt was confirmed by UV-vis measurement (Fig. S45). The incomplete loading is consistent with the limited solubility of the free-pocket cage in MeCN and the heterogeneous nature of the process, in which cation exchange occurs at the solid–solution interface. Together, these results demonstrate that sodium ions supplied from an organic dye salt can be incorporated into the sulfonate binding pocket under post-synthetic conditions, yielding a porous salt that combines cage-derived porosity with dye-based optical functionality.

To demonstrate that the porous cage scaffold can be paired with discrete transition-metal complexes of potential catalytic relevance, we next examined porous salt formation using Li_2PdCl_4 as a Li^+-balanced anion source. Treatment of the free-pocket cage with Li_2PdCl_4 afforded a grey–brown solid that retained porosity to CO_2 but not to N_2. XPS analysis revealed a Pd : Zr ratio of approximately 1 : 9 (Fig. 4a), consistent with

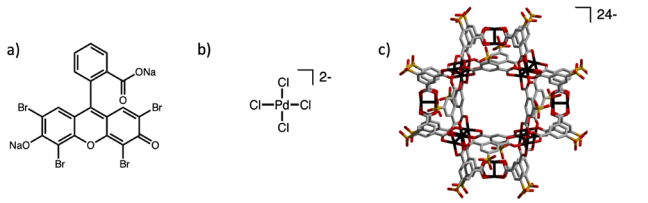

Fig. 3 Structures of Na^+/Li^+ bearing complexes. (a) Eosin Y disodium salt. (b) Li_2PdCl_4. (c) $[Mo_{24}(5\text{-}SO_3\text{-}bdc)_{24}]^{24-}$. Mo: black, O: red, C: grey, S: yellow.

formation of a charge-balanced porous salt formulated as $[Li_2PdCl_4][free\text{-}pocket]$, in which Li^+ occupies the tri-sulfonate binding pocket. The selective retention of CO_2 accessibility indicates that incorporation of the Pd complex modifies the pore environment while still allowing for the adsorption of smaller gases, highlighting the ability of this approach to decouple porosity from the introduction of metal-centered functionality (Fig. 4d).

Finally, we extended this strategy to the assembly of porous salts from two charged coordination cages using a cuboctahedral molybdenum-based cage $Li_{24}[Mo_{24}(5\text{-}SO_3\text{-}bdc)_{24}]$. This Mo cage, composed of twelve Mo–Mo paddlewheel units bridged by twenty-four 5-SO_3-bdc ligands with Li^+ counterions, is structurally and chemically rich but intrinsically nonporous to N_2 in the solid state (Fig. 3c).

Combination of the free-pocket Zr cage with $Li_{24}[Mo_{24}(5\text{-}SO_3\text{-}bdc)_{24}]$ afforded a charge-balanced porous salt formulated as $Li_{14}[(Zr_3(\mu_3\text{-}O)(\mu_2\text{-}OH)_3Cp_3)_3(5\text{-}SO_3\text{-}bdc)_4Li]_{10}[Mo_{24}(5\text{-}SO_3\text{-}bdc)_{24}]$, as determined from Zr : Mo ratios obtained by XPS and

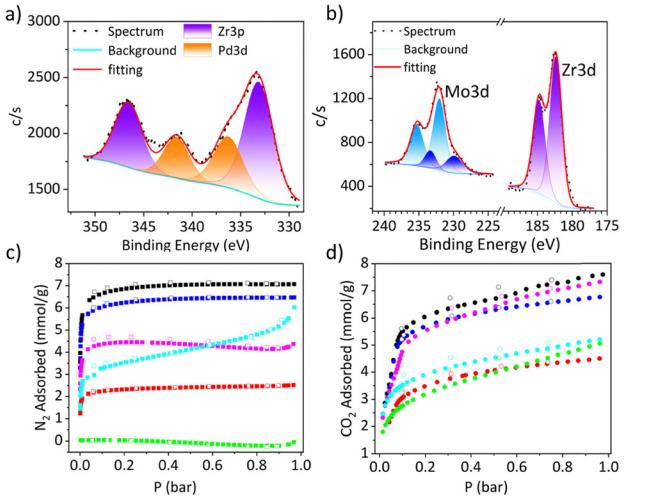

Fig. 4 (a) XPS spectra of Pd 3d with deconvolution for salt made from free-pocket cage and Li_2PdCl_4. (b) XPS spectra of Zr 3d and Mo 3d for salt made from free-pocket cage and $Li_{24}[Mo_{24}(5\text{-}SO_3\text{-}bdc)_{24}]$ cage. For all XPS spectra, binding energy was calibrated to C 1s (284.80 eV). N_2 isotherms (c) at 77 K and CO_2 isotherms (d) at 195 K of Na-bound cage (black), Li-bound (red), free-pocket cage (blue), salt made from free-pocket cage and Eosin Y dye (magenta), salt made from free-pocket cage and Li_2PdCl_4 (green), and salt made from free-pocket cage and $Li_{24}[Mo_{24}(5\text{-}SO_3\text{-}bdc)_{24}]$ cage (cyan). Closed and open symbols represent adsorption and desorption, respectively.

corroborated by ^{1}H NMR spectroscopy (Fig. 4b and Fig. S28). In contrast to $Li_{24}[Mo_{24}(5\text{-}SO_3\text{-}bdc)_{24}]$ alone, the resulting salt exhibits moderate N_2 porosity with a BET surface area of 289 m^2 g^{-1} (Fig. 4c), demonstrating that porosity is imparted by the Zr cage scaffold while preserving accessibility to the Mo-based paddlewheel units. The porous salt also displays moderate O_2 uptake of 0.31 mmol g^{-1} at 298 K, approaching the value expected for one oxygen per Mo_2 paddlewheel unit (Fig. S43).

In conclusion, we demonstrate that a sulfonate-functionalized zirconium coordination cage can serve as a porous scaffold for assembling porous salts through solid-state binding of alkali metal cations. Sodium and lithium ions act as charge-balancing connectors that enable pairing of the porous cage with functionally rich counter-anions, including optically active dyes, transition-metal complexes, and charged coordination cages. In each case, the cage provides permanent porosity while the counter-anion introduces complementary optical, chemical, or gas-binding functionality. This modular, charge-driven approach offers a general strategy for transforming otherwise nonporous or functionally isolated species into accessible porous materials.

The authors gratefully acknowledge financial support from the National Science Foundation (2421967) and Indiana University. Support for the acquisition of the Bruker Venture D8 diffractometer through the Major Scientific Research Equipment Fund from the President of Indiana University and the Office of the Vice President for Research is gratefully acknowledged.

Conflicts of interest

There are no conflicts to declare.

Data availability

The data supporting this article have been included as part of the supplementary information (SI). Supplementary information: adsorption isotherms, crystallographic information, spectroscopic data. See DOI: https://doi.org/10.1039/d6cc00930a.

CCDC 2475056, 2475059 and 2475058 contain the supplementary crystallographic data for this paper.[38a–c]

References

1 N. Hosono and S. Kitagawa, *Acc. Chem. Res.*, 2018, **51**, 2437–2446.
2 A. J. Gosselin, C. A. Rowland and E. D. Bloch, *Chem. Rev.*, 2020, **120**, 8987–9014.
3 K. Yazaki, Y. Sei, M. Akita and M. Yoshizawa, *Chem. – Eur. J.*, 2016, **22**, 17557–17561.
4 Z. Su, K.-K. Liu, Y.-Q. Xu, B. Yan, S. Wang, Z.-J. Guan, Y. Zou and Y. Fang, *Angew. Chem., Int. Ed.*, 2025, **64**, e202420945.
5 M. R. Dworzak, C. A. Rowland, G. P. A. Yap and E. D. Bloch, *CrystEngComm*, 2022, **24**, 6315–6319.
6 J. Hoq, M. R. Dworzak, D. Dissanayake, R. X. Skalla, N. Yamamoto, G. P. A. Yap and E. D. Bloch, *Chem. Commun.*, 2025, **61**, 1641–1644.
7 G. Li, Z. Du, C. Wu, Y. Liu, Y. Xu, R. Lavendomme, S. Liang, E.-Q. Gao and D. Zhang, *Nat. Commun.*, 2025, **16**, 546.
8 A. B. Grommet, J. B. Hoffman, E. G. Percástegui, J. Mosquera, D. J. Howe, J. L. Bolliger and J. R. Nitschke, *J. Am. Chem. Soc.*, 2018, **140**, 14770–14776.
9 B. Le Ouay, M. Tokiwa, R. Ohtani and M. Ohba, *Chem. Mater.*, 2025, **37**, 3414–3422.
10 A. M. Antonio, M. R. Dworzak, K. J. Korman, G. P. A. Yap and E. D. Bloch, *Chem. Mater.*, 2022, **34**, 10823–10831.
11 M. M. Deegan, A. M. Antonio, K. J. Korman, A. A. Ezazi, K. Korathotage, M. N. Morey, J. Hoq, D. Dissanayake, D. D. Fernando, G. P. A. Yap, D. C. Powers and E. D. Bloch, *Chem. Mater.*, 2025, **37**, 2404–2417.
12 A. J. Gosselin, G. E. Decker, A. M. Antonio, G. R. Lorzing, G. P. A. Yap and E. D. Bloch, *J. Am. Chem. Soc.*, 2020, **142**, 9594–9598.
13 L.-H. Wu, S.-N. Liu, B.-X. Zhou, S.-L. Cai, W.-G. Zhang and S.-R. Zheng, *Chem. Commun.*, 2023, **59**, 9118–9121.
14 A. Sur, J. D. Simmons, A. A. Ezazi, K. J. Korman, S. Sarkar, E. T. Iverson, E. D. Bloch and D. C. Powers, *J. Am. Chem. Soc.*, 2023, **145**, 25068–25073.
15 A. J. Gosselin, A. M. Antonio, K. J. Korman, M. M. Deegan, G. P. A. Yap and E. D. Bloch, *J. Am. Chem. Soc.*, 2021, **143**, 14956–14961.
16 W.-Y. Lan, D.-S. Wei, W.-X. Duan, X.-H. Li, Z. Sun, Y.-T. Zhang, N. Lv, H.-H. Yu and S.-B. Li, *J. Mol. Struct.*, 2025, **1346**, 143227.
17 C. Perona-Bermejo, R. Vismara, N. M. Padial, N. Almora-Barrios, C. R. Maldonado, T. J. Bandosz, P. Garrido-Barros, F. J. Carmona and J. A. R. Navarro, *Adv. Funct. Mater.*, 2024, **34**, 2405785.
18 B. Le Ouay, R. Minami, P. K. Boruah, R. Kunitomo, Y. Ohtsubo, K. Torikai, R. Ohtani, C. Sicard and M. Ohba, *J. Am. Chem. Soc.*, 2023, **145**, 11997–12006.
19 K. J. Korman, M. R. Dworzak, G. P. A. Yap and E. D. Bloch, *Small*, 2023, **19**, 2370226.
20 Y.-L. Lu, Y.-P. Wang, K. Wu, M. Pan and C.-Y. Su, *Acc. Chem. Res.*, 2024, **57**, 3277–3291.
21 H. A. Silva, B. S. Whitehead, C. D. Hastings, C. K. Tiwari, W. W. Brennessel and B. R. Barnett, *Organometallics*, 2024, **43**, 2599–2607.
22 Y.-P. He, L.-B. Yuan, J.-S. Song, G.-H. Chen, Q. Lin, C. Li, L. Zhang and J. Zhang, *Chem. Mater.*, 2018, **30**, 7769–7775.
23 C. K. Ng, R. W. Toh, T. T. Lin, H.-K. Luo, T. S. A. Hor and J. Wu, *Chem. Sci.*, 2019, **10**, 1549–1554.
24 W.-J. Shi, D. Liu, X. Li, S. Bai, Y.-Y. Wang and Y.-F. Han, *Chem. – Eur. J.*, 2021, **27**, 7853–7861.
25 B.-X. Jiang, S.-B. Li, J. Li, T.-T. Xu, N. Lv and Y.-T. Zhang, *Inorg. Chem. Commun.*, 2024, **165**, 112581.
26 J. Jiao, C. Tan, Z. Li, Y. Liu, X. Han and Y. Cui, *J. Am. Chem. Soc.*, 2018, **140**, 2251–2259.
27 K. Harris, Q.-F. Sun, S. Sato and M. Fujita, *J. Am. Chem. Soc.*, 2013, **135**, 12497–12499.
28 D. J. Bell, L. S. Natrajan and I. A. Riddell, *Coord. Chem. Rev.*, 2022, **472**, 214786.
29 Y. Wang, Y. Zhang, Z. Zhou, R. T. Vanderlinden, B. Li, B. Song, X. Li, L. Cui, J. Li, X. Jia, J. Fang, C. Li and P. J. Stang, *Nat. Commun.*, 2020, **11**, 2727.
30 G. Liu, M. Zeller, K. Su, J. Pang, Z. Ju, D. Yuan and M. Hong, *Chem. – Eur. J.*, 2016, **22**, 17345–17350.
31 M. Maity, P. Howlader and P. S. Mukherjee, *Cryst. Growth Des.*, 2018, **18**, 6956–6964.
32 C. Ji, W. Wang, E.-S. M. El-Sayed, G. Liu, Y. Si, K. Su, Z. Ju, F. Wu and D. Yuan, *Appl. Catal., B*, 2021, **285**, 119782.
33 J. Zhu, Z.-Y. Liu, S.-B. Li, H. Huang, B.-X. Jiang and Y.-T. Zhang, *CrystEngComm*, 2022, **24**, 475–478.
34 W.-L. Jiang, B. Huang, X.-L. Zhao, X. Shi and H.-B. Yang, *Chem*, 2023, **9**, 2655–2668.
35 W. J. Ramsay, F. J. Rizzuto, T. K. Ronson, K. Caprice and J. R. Nitschke, *J. Am. Chem. Soc.*, 2016, **138**, 7264–7267.
36 S. Du, X. Yu, G. Liu, M. Zhou, E. M. EI-Sayed, Z. Ju, K. Su and D. Yuan, *Cryst. Growth Des.*, 2021, **21**, 692–697.
37 E. M. El-Sayed, Y. D. Yuan, D. Zhao and D. Yuan, *Acc. Chem. Res.*, 2022, **55**, 1546–1560.
38 (*a*) CCDC 2475056: Experimental Crystal Structure Determination, 2026, DOI: 10.5517/ccdc.csd.cc2p2hjt; (*b*) CCDC 2475059: Experimental Crystal Structure Determination, 2026, DOI: 10.5517/ccdc.csd.cc2p2hmx; (*c*) CCDC 2475058: Experimental Crystal Structure Determination, 2026, DOI: 10.5517/ccdc.csd.cc2p2hlw.